INTEK: Jurnal Penelitian
Vol. 13, No. 2, pp. 11-23, October 2026
DOI: https://doi.org/10.31963/intek.v13i2.6702

Tuning the Structural and Textural Properties of H-ZSM-5 through Si/Al Molar Ratio Variation

Fazlena Hamzah[1,a], Ridhawati Thahir[2,*,b], Joice Manga[2,c], Mimin Septiani[2,d], and Dian Ranggina[2,e]
[1] Faculty of Chemical Engineering, Universiti Teknologi MARA, UiTM Shah Alam, 40450 Shah Alam, Malaysia
[2] Chemical Engineering Department, Politeknik Negeri Ujung Pandang, Jl. Perintis Kemerdekaan Km. 10, Makassar, 90245, Indonesia

[a] fazlena@uitm.edu.my, *,[b] ridha331@poliupg.ac.id (Corresponding author), [c] joicemanga@poliupg.ac.id, [d] miminseptiani@poliupg.ac.id, [e] dian.ranggina.dr@poliupg.ac.id

Article Info

Keywords: ZSM-5; MFI Structural; Microporous; Si/Al molar ratio

Received. : 13 09 2026
Revised form : 05 10 2026
Accepted. : 11 10 2026
Published. : 30 10 2026

Abstract

ZSM-5 is a typical and widely utilised zeolite of MFI type. The Si/Al molar ratio, controlling the framework acidity and subsequent textural architecture, strongly influences its catalytic and adsorptive performance. The present work examined the effect of the Si/Al molar ratio on the structural and textural properties of ZSM-5 synthesised at a fixed crystallisation temperature. Tetrapropyl ammonium hydroxide (TPAOH) was the structure directing agent and tetraethyl orthosilicate (TEOS) the silica source. Two ZSM-5 samples with Si/Al molar ratios of 80 and 120 ("Z-T80-TE-170" and "Z-T120-TE-170") were hydrothermally synthesised at 170°C. The samples were characterized by XRD, FTIR, and N_2 physisorption. The XRD patterns of both samples showed the characteristic orthorhombic MFI reflections at $2\theta \approx 7–9°$ [(101)/(200)] and 23–24° [(332)/(303)], indicating that the pentasil framework was retained at both compositions. FTIR spectra supported the formation of the MFI structure through the double five-membered ring (D5R) vibration 550 cm^{-1}, together with the framework bands at 1080, 800, and 450 cm^{-1}. Increasing the Si/Al ratio from 80 to 120 raised the BET surface area from 323.5 to 566.7 m^2/g and the total pore volume from 0.485 to 0.822 cm^3/g, while the DFT-derived pore width 3.54 to 4.89 nm. These results indicate that a higher Si/Al ratio at constant crystallization temperature is accompanied by enhanced intercrystalline mesoporosity, while the MFI framework remains intact. These findings offer a basis for tuning the Si/Al ratio to design ZSM-5 with improved pore accessibility for adsorption and catalytic applications.

1. Introduction

Zeolites are crystalline microporous aluminosilicates that have received considerable attention for their well-defined framework topologies, tunable acidity, hydrothermal stability, and molecular-sieving properties, which underpin their use in catalysis, adsorption, separation, and environmental applications [1], [2], [3], [4], [5]. Among the synthetic zeolites, ZSM-5 is of particular interest because of the MFI structure with interconnected 10-membered-ring channels, combine shape-selectivity, diffusion characteristics, and high structural stability [6]; it is also the standard reference material designated by the International Zeolite Association for the MFI framework

The hydrothermal synthesis of ZSM-5 proceeds through nucleation and crystal growth of an aluminosilicate framework from reactive Si- and Al-containing species in an alkaline solution containing an organic structure-directing agent (SDA) [7], [8], [9]. Crystallization depends strongly on the synthesis variables, including the composition and concentration of the silicon and aluminum sources, alkalinity, water content, SDA

concentration, aging, crystallization temperature, and crystallization time [10], [11], and previous studies have shown that these variables determine the nucleation kinetics, crystal development, morphology, and aluminum distribution of the resulting ZSM-5 framework. Among these factors, the Si/Al ratio is particularly critical because substituting aluminum into the silicate framework alters the framework composition and, consequently, the physicochemical properties of ZSM-5, including crystallinity, morphology, pore structure, surface acidity, and the relative contributions of the external and internal surfaces [10], [12], [13]. Recent work has demonstrated that the pore shape, morphology, acidity, and crystallinity of MFI zeolites can be effectively tuned by adjusting the Si/Al ratio in the synthesis gel.

The Si/Al composition and crystallization are not always linearly correlated. Al-containing species may alter nucleation and crystal-growth kinetics, while incorporating Al into tetrahedral framework sites may change XRD and infrared spectrum features. XRD patterns have shown that the crystallization behavior of ZSM-5 is highly dependent on the Si/Al composition and crystallization duration, with larger aluminum levels requiring longer crystallization times to achieve similar structural development [14]. Structural features of ZSM-5 can be assessed using complementary spectroscopic and diffraction techniques. XRD is direct evidence for the crystalline MFI phase, whereas FTIR gives information on framework vibrations.

Characteristic ZSM-5 infrared bands are generally observed near 450–470, 550–560, 790–800, 1050–1100, and approximately 1220–1230 cm^{-1}. In particular, the band near 550–560 cm^{-1} is associated with the double five-membered-ring structural unit, while bands in the 1050–1100 cm^{-1} region are related to T–O–T framework vibrations. Textural characterization provides an additional means of evaluating the consequences of Si/Al variation. N_2 physisorption can resolve changes in specific surface area, pore volume, and pore-size distribution resulting from differences in framework development and particle aggregation. Recent studies have shown that ZSM-5 materials can exhibit substantial differences in BET surface area and mesopore contribution, depending on synthesis conditions and framework modification [8], [12], [15].

Despite extensive research on Si/Al-dependent ZSM-5 synthesis, many studies vary several synthesis parameters simultaneously, making it difficult to separate the contribution of composition from that of hydrothermal treatment. A controlled comparison at a fixed crystallization temperature therefore provides a useful approach for isolating the effect of the Si/Al ratio. In the present work, ZSM-5 samples with nominal Si/Al ratios of 80 and 120 were synthesized under the same hydrothermal temperature of 170°C. The resulting materials were investigated by XRD, FTIR, and N_2 physisorption using BET, BJH, DFT, and t-plot analyses.

The novelty of this work lies in three aspects. First, the Si/Al molar ratio is the only synthesis variable that is changed: the silica source (TEOS), the structure-directing agent (TPAOH), the gel preparation and the crystallization temperature of 170 °C are held constant for both samples, so the structural and textural differences reported here can be attributed to framework composition alone rather than to the combined action of several synthesis parameters, as is the case in studies where composition and hydrothermal treatment are varied together. Second, the structural response and the textural response are deliberately separated by using diffraction, vibrational and physisorption evidence on the same pair of samples. XRD retains the characteristic orthorhombic MFI reflections at $2\theta \approx 7–9°$ and 23–24° and FTIR retains the double five-membered-ring vibration near 550 cm^{-1} at both compositions, whereas N_2 physisorption shows a large change in texture, with the BET surface area rising from 323.5 to 566.7 $m^2 g^{-1}$, the total pore volume from 0.485 to 0.822 $cm^3 g^{-1}$ and the DFT-derived pore width from 3.54 to 4.89 nm. The result therefore demonstrates that the pore accessibility of ZSM-5 can be almost doubled without altering the MFI framework itself, which is a practical design conclusion rather than a general observation that the Si/Al ratio matters. Third, the pore architecture is resolved by applying BET, BJH, DFT and t-plot analyses to the same isotherms, which allows the additional surface

area and pore volume to be attributed to intracrystalline mesoporosity developing between crystallites rather than to a modification of the intrinsic micropore system of the MFI channels.

The objective of this work was therefore to clarify how increasing the Si/Al molar ratio from 80 to 120 affects the development of the MFI framework and the associated textural properties of ZSM-5. Particular attention was given to the relationship between XRD features, framework vibrations, surface area, pore volume, and pore-size characteristics.

2. Research Methodology

2.1. Materials and Methods

Tetraethyl orthosilicate (TEOS, Sigma-Aldrich) was used as the silicon precursor, aluminum hydroxide [Al (OH)$_3$, Merck] as the aluminum source, and tetrapropylammonium hydroxide (TPAOH, 40%, Sigma-Aldrich) as the organic structure-directing agent. Deionized water was used as the solvent. The synthesis compositions were adjusted to nominal Si/Al molar ratios of 80 and 120.

2.2. Synthesis of H-ZSM-5

ZSM-5 samples with Si/Al ratios of 80 and 120, designated Z-T80-TE and Z-T120-TE, respectively, were synthesized by a modified hydrothermal method based on previously reported procedures for TEOS–TPAOH-containing ZSM-5 systems [1], [16], [17] with TPAOH as the structure-directing agent and TEOS as the silicon source, as shown in Figure 1. For the synthesis of the Z-T80-TE and Z-T120-TE samples, 0.097 and 0.065 g of Al (OH)$_3$ were added to 10.5 mL of TPAOH, respectively, and the mixture was agitated at 30 °C and 300 rpm until homogeneous (solution A). Separately, 0.166 g NaOH was diluted in 20 mL distilled water, and then 10.5 mL of TPAOH was added; the mixture was agitated at 400 rpm for 10 min.

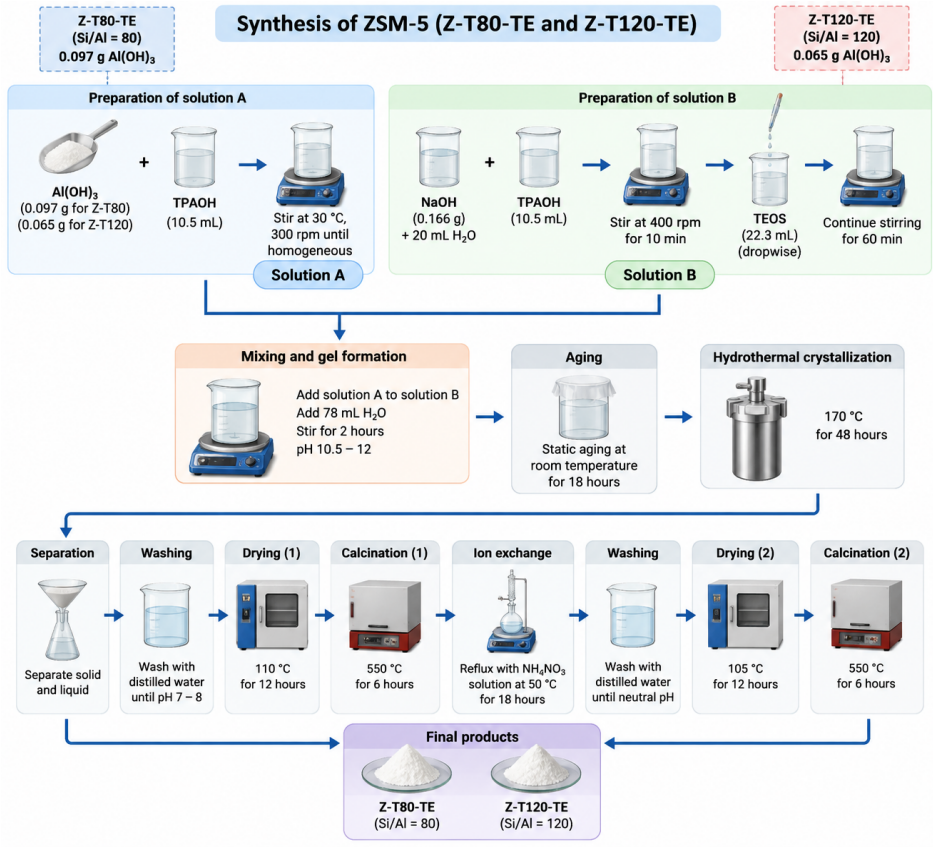


FIGURE 1. Synthesis pathway of H-ZSM-5

Subsequently, 22.3 mL of TEOS was added dropwise, and the mixture was stirred for 60 min to obtain solution B. The two solutions were combined, and 78 mL of distilled water was introduced. The resulting gel was agitated for 2 h, adjusted to pH 10.5- 12, and aged statically at room temperature for 18 h. Hydrothermal crystallization was then carried out at 170ºC for 48 h. The solid product was filtered, washed with distilled water to pH 7–8, and dried at 110°C for 12 h. The dry Na-ZSM-5 product was calcined at 550°C for 6 h. The calcined material was refluxed with NH_4NO_3 solution at 50°C for 18 h, washed with distilled water until neutral pH, and dried at 105°C for 12 h. Finally, the material was calcined again at 550°C for 6 h to obtain the H-ZSM-5) product, designated Z-T80-TE and Z-T120-TE.

2.3. Characterization of ZSM-5

Powder XRD measurements were performed on a Shimadzu Maxima-X XRD-7000 diffractometer using Cu Kα radiation at 40 kV and 30 mA, with scans collected over a 2θ range of 5–70°, and a step size of 0.020°. These conditions are directly documented in the uploaded XRD files. The diffraction patterns were used to identify the crystalline phase and to evaluate the development of the MFI framework. FTIR spectra were recorded on a Shimadzu 8400S spectrometer over the mid-infrared region to identify the characteristic vibrations associated with the aluminosilicate framework, with particular attention given to the T–O–T vibration region and the characteristic double five-membered-ring vibration near 550 cm^{-1}. N_2 adsorption–desorption measurements were carried out on an ANTON Paar NOVA Touch 4LX instrument to determine BET (Brunauer-Emmett-Teller) specific surface area, total pore volume, and pore-size characteristics. Pore-size distributions were evaluated by BJH (Barrett–Joyner–Halenda) and DFT (Density Functional Theory) analyses, while t-plot analysis was employed to assess the microporosity contribution and external surface area.

3. Results and Discussion

3.1. XRD analysis: development of the MFI framework

Figure 2a shows the XRD patterns of Z-T80-TE-170 and Z-T120-TE-170. The two samples exhibited similar diffraction patterns over the measured 2θ range of 5-70°, indicating that the same main crystalline phase formed in both cases. The characteristic reflections of the MFI-type ZSM-5 framework were clearly observed in the magnified region of 5–35° (Figure 2b and Table 1), particularly at approximately ~7.9–8.0°, ~8.9°, and ~23–24°, which were attributed to the (101), (200), (332), and (303) crystallographic planes [6], [16], [18]. The presence of these characteristic reflections indicates that a successful development of the ZSM-5 crystalline framework occurred in both samples. Interestingly, Z-T120-TE-170 shows higher diffraction intensities in a few typical MFI reflections, especially in the 23° region, suggestive of a relatively stronger structural ordering/crystallinity in comparison to Z-T80-TE-170. The difference is probably related to the increased Si/Al ratio, affecting the chemical environment during nucleation and crystal growth, and favoring the formation of a more siliceous MFI framework.

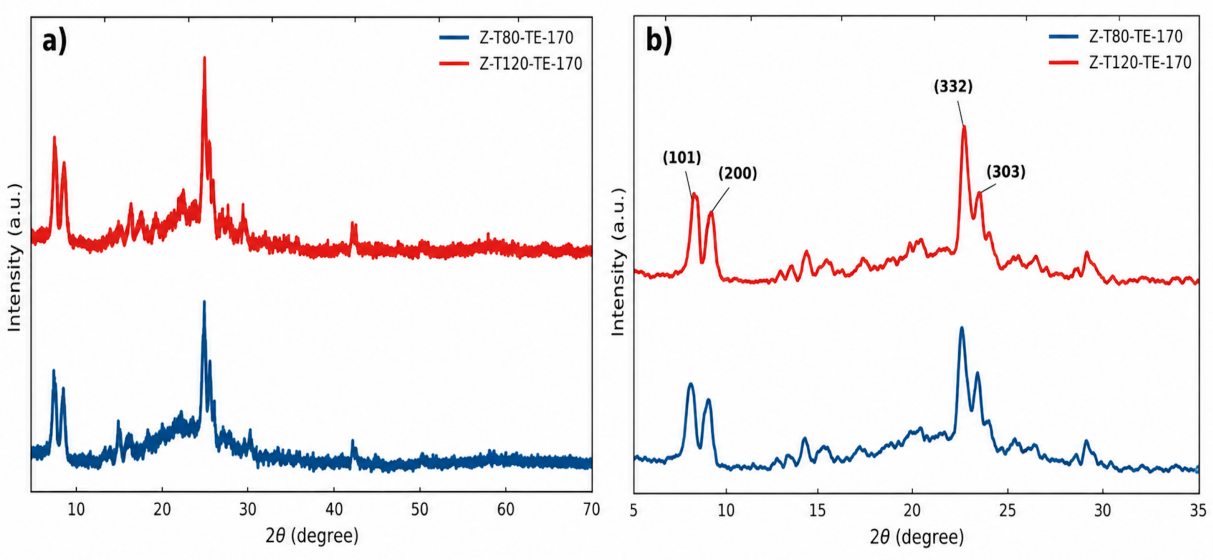


FIGURE 2. Powder XRD analysis of ZSM-5

The more intense diffraction signals linked to MFI found for the Z-T120-TE-170 sample indicate a better formation of the crystalline MFI phase under the specified synthesis conditions. This is consistent with recent studies highlighting the effect of the Si/Al ratio on MFI crystallization and structure evolution. However, the increase in peak intensity should not be overinterpreted as a direct quantitative indicator of crystallinity.

TABLE 1. Principal XRD reflections based on JCPDS No. 00-044-0003 for MFI-type ZSM-5

2θ (°) Z-T80-TE-170	**2θ (°) Z-T120-TE-170**	**Assigned hkl**
7.90	7.98	(101)
8.94	8.94	(200)
23.20	23.20	(332)
23.96	24.06	(303)

A comprehensive analysis of relative crystallinity would need integration over a specific reflection region and normalization to an appropriate reference. Thus, XRD results in this study are discussed mostly as an indication of changes in MFI structural evolution rather than absolute percentages of crystallinity.

3.2. FTIR analysis

The FTIR spectra provided complementary evidence for the formation of the aluminosilicate framework. As shown in Figure 3, characteristic ZSM-5 vibrations are expected near 450–470 cm^{-1}, 550–560 cm^{-1}, 790–800 cm^{-1}, 1050–1100 cm^{-1}, and approximately 1220–1230 cm^{-1}. The band near 550–560 cm^{-1} is particularly associated with the double five-membered-ring structural unit characteristic of the MFI topology. For the present samples, the framework-related bands observed in the FTIR spectra are consistent with the formation of an aluminosilicate ZSM-5 framework. The presence of the characteristic double five-membered-ring (D5R) vibration together with the T–O–T stretching bands supports the XRD identification of MFI-type ZSM-5. The FTIR results should therefore be interpreted as complementary rather than independent proof of crystallinity. Together, characteristic XRD reflections and MFI-sensitive FTIR bands provide stronger evidence of successful framework formation than either technique alone.

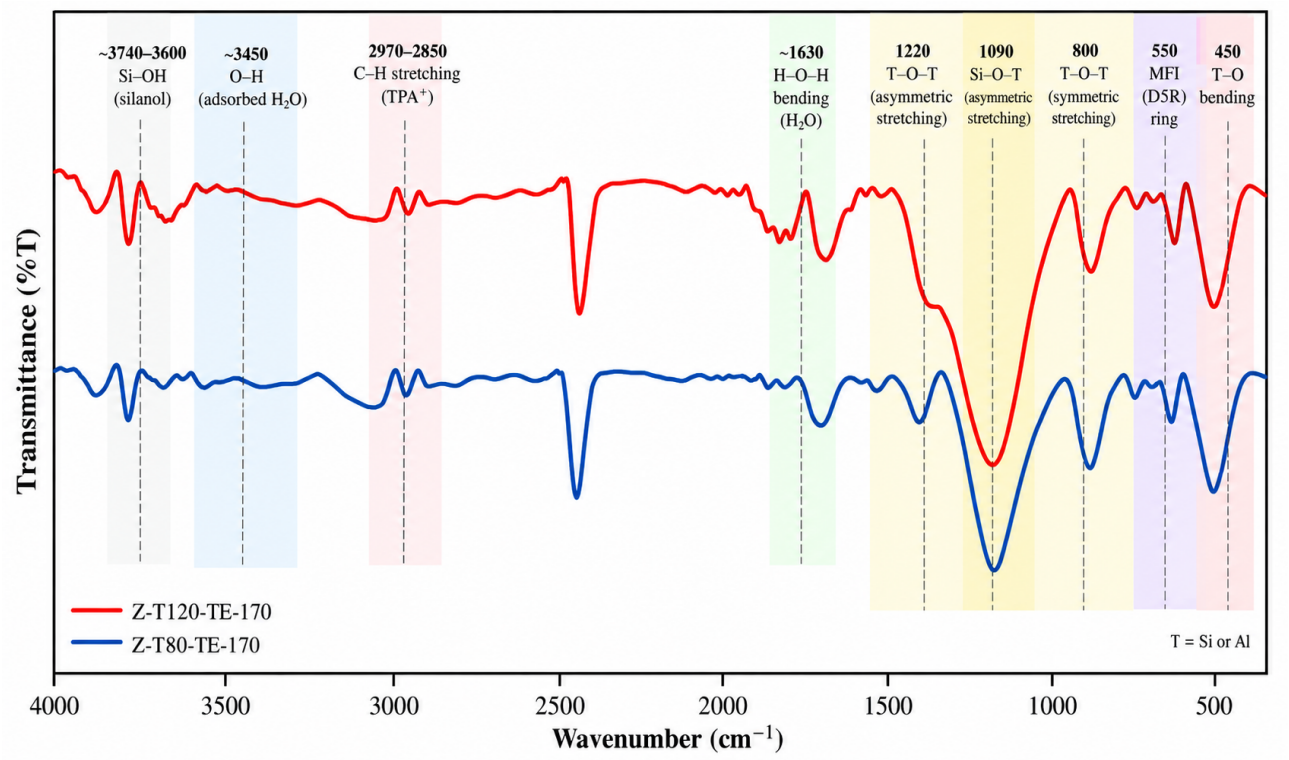


FIGURE 3. FTIR spectra of the MFI-type ZSM-5

Both samples presented the full set of framework vibration bands characteristic of the MFI-type zeolite structure, confirming successful crystallization of ZSM-5 at 170°C irrespective of the Si/Al ratio studied. These bands arise from internal vibrations of the $(Si\text{-}Al)O_4$ tetrahedra that constitute the zeolite framework, and their number, position, and relative intensity collectively serve as a structural fingerprint that complements the long-range periodicity information obtained from XRD [19], [20]. Among these, the band near 550–580 cm^{-1} is of

particular diagnostic value, as it arises specifically from the vibration of the double five-membered-ring (5-1) secondary building units that link the pentasil chains characteristic of the MFI framework topology, and is therefore widely used in the zeolite literature to distinguish MFI-type materials (ZSM-5, silicalite-1) from other framework types as well as from X-ray-amorphous silica or aluminosilicate phases that lack this specific ring connectivity [19]. In the present samples, this band is clearly resolved at 561.3 cm^{-1} for Z-T80-TE-170 (Si/Al = 80) and at 559.4 cm^{-1} for Z-T120-TE-170 (Si/Al = 120), a difference of less than 2 cm^{-1}, which is within the typical spectral resolution of the measurement and therefore not considered a meaningful shift.

The near-identical position of this band in both samples confirms that a well-developed, five-membered-ring-containing MFI framework has formed in both cases, and that this particular structural feature is essentially insensitive to the Si/Al ratio variation applied here. This conclusion was further supported by two additional framework bands. The T–O bending mode, observed at 459.1 cm^{-1}, is identical between the two samples to within the resolution of the instrument, indicating that the local bending motion of the tetrahedral framework oxygen atoms is unaffected by the change in aluminium content over this range. Similarly, the secondary framework band near 633–635 cm^{-1} associated with additional ring-vibration modes of the pentasil structure showed only a negligible shift (approximately 2 cm^{-1}) between the two samples. Taken together, the consistent position of the 550–580 cm^{-1}, 459 cm^{-1}, and 633–635 cm^{-1} bands across both samples indicates that the overall MFI topology, and specifically the connectivity of its characteristic five-membered-ring building, is preserved across the Si/Al ratio range studied, with the compositional variation instead manifesting primarily in the internal T–O–T stretching region discussed below [18], [19].

The most significant difference between the two samples is seen in the asymmetric internal T-O-T stretching band, which is shifted from 1057.0 cm^{-1} for Z-T80-TE-170 to 1072.5 cm^{-1} for Z-T120-TE-170, a blue shift of ~15 cm^{-1}. This trend is consistent with the established correlation between framework Si/Al ratio and T-O-T bond vibration frequency: as the Si/Al ratio increases, the proportion of Si-O-Si linkages increases relative to the longer and weaker Si-O-Al linkages, and the asymmetric stretching frequency shifts to a higher wavenumber [20]. The symmetric T-O-T stretch, in contrast, showed only a minor shift, from 806.3 to 804.3 cm^{-1}, the fact that this mode is often less sensitive to Al substitution than the asymmetric mode. Also, a change is detected in the hydroxyl region where the band presently assigned to bridging Si-OH-Al (Brønsted acid) hydroxyl groups shifts from 3634.0 cm-1 in the Z-T80-TE-170 sample to 3612.8 cm^{-1} in Z-T120-TE-170. The previous study value for the bridging hydroxyl stretch in H-ZSM-5 most often cited is close to 3610 cm^{-1}, and the position of this band is known to be sensitive to the identity and local environment of the tetrahedral framework atom to which the hydroxyl is bridged, with a known correlation between bridging-OH wavenumber and Brønsted acid strength [3], [21]. The result for Z-T120-TE-170 (3612.8 cm^{-1}) is around the normal position; however, the value for Z-T80-TE-170 (3634.0 cm^{-1}) is clearly higher. As with all spectra in this series, the sharp signal about 2355-2357 cm^{-1} is an artifact arising from the asymmetric stretch of ambient CO_2 and is not a sample vibrational mode and should be omitted from structural interpretation.

The FTIR results in the overall sample demonstrate that raising the Si/Al ratio from 80 to 120 at a constant crystallization temperature of 170 °C does not affect the formation of the MFI framework, but does induce a measurable systematic shift in the internal asymmetric T–O–T stretching frequency and a significant difference in the bridging hydroxyl position, both of which are consistent with lower framework aluminum incorporation at the higher Si/Al ratio.

3.3. Effect of Si/Al ratio on textural properties

The N_2 physisorption data (Table 1) showed a significant difference between Z-T80-TE-170 and Z-T120-TE-170 samples. The cumulative surface area and pore volume plots reveal a notable difference in the textural evolution of Z-T80-TE-170 and Z-T120-TE-170. However, the increase in the Si/Al ratio to 120 significantly improved both characteristics, indicating that Z-T120-TE-170 attained 440–450 m^2/g and 0.87–0.89 cm^3/g, respectively. Therefore, the total surface area and pore volume increased from approximately 70 percent and 66%, respectively. The comparative pore size distributions further indicate that Z-T120-TE-170 has a more established secondary pore network in the nanometer range. This effect is common for the more substantial hierarchical pore design of intrinsic microporous ZSM-5 channels and secondary mesoporosity. Such hierarchical design is invaluable for enhancing molecular transport, as the secondary mesopores offer more diffusion channels to the microporous domains. Such behavior has been shown for hierarchical ZSM-5, where secondary mesoporosity enhances the exterior surface area and mesopore volume while decreasing the diffusion limitations of the normal MFI micropore system.

TABLE 2. Nitrogen physisorption data for ZSM-5 samples

Parameter	Sample	
	Z-T80-TE-170	**Z-T120-TE-170**
BET surface area ($m^2\ g^{-1}$)	323.50	566.73
BET pore volume ($cm^3\ g^{-1}$)	0.4849	0.8217
BET pore diameter (nm)	6.00	5.80
DFT surface area ($m^2\ g^{-1}$)	257.93	446.54
DFT pore volume ($cm^3\ g^{-1}$)	0.5373	0.8717
DFT pore width (nm)	3.54	4.89
t-plot micropore area ($m^2\ g^{-1}$)	15.70	0
t-plot micropore volume ($cm^3\ g^{-1}$)	0.0035	0
t-plot external surface area ($m^2\ g^{-1}$)	308.33	117.98
Average pore diameter, BET method (nm)	5.99	5.80

The BET surface area increased from 323.50 to 566.73 m^2/g as the nominal Si/Al ratio was raised from 80 to 120 (Table 2; Figure 6). Rather than being accompanied by a proportional increase in average pore diameter, the higher Si/Al ratio produces a substantial increase in accessible surface area and pore volume while the average pore diameter remains approximately similar. This suggests that the principal textural effect of increasing Si/Al from 80 to 120 is not simply enlargement of individual pores. Instead, it is more appropriately interpreted as enhanced development or accessibility of the porous network. The literature supports the sensitivity of MFI porosity to Si/Al composition. Manipulation of the Si/Al ratio in the synthesis gel has been shown to modify mesostructure, morphology, acidity, and crystallinity.

Figure 4 provides an overview of the BJH pore diameters for both samples (~2.26-2.30 nm) sit at the lower boundary of the method's reliable detection range (BJH is generally considered accurate for pores $\gtrsim$2 nm), so this specific narrow value should be reported with the caveat that it may partly reflect the lower cutoff of the method's applicable range rather than a sharply defined pore population. Taken together, the BET/BJH/DFT results indicate that while the MFI crystalline framework itself is structurally similar between

the two Si/Al ratios, the overall pore architecture, total surface area, mesopore volume, and mode pore width differs substantially, with Z-T120-TE-170 exhibiting a much more developed mesoporous texture.

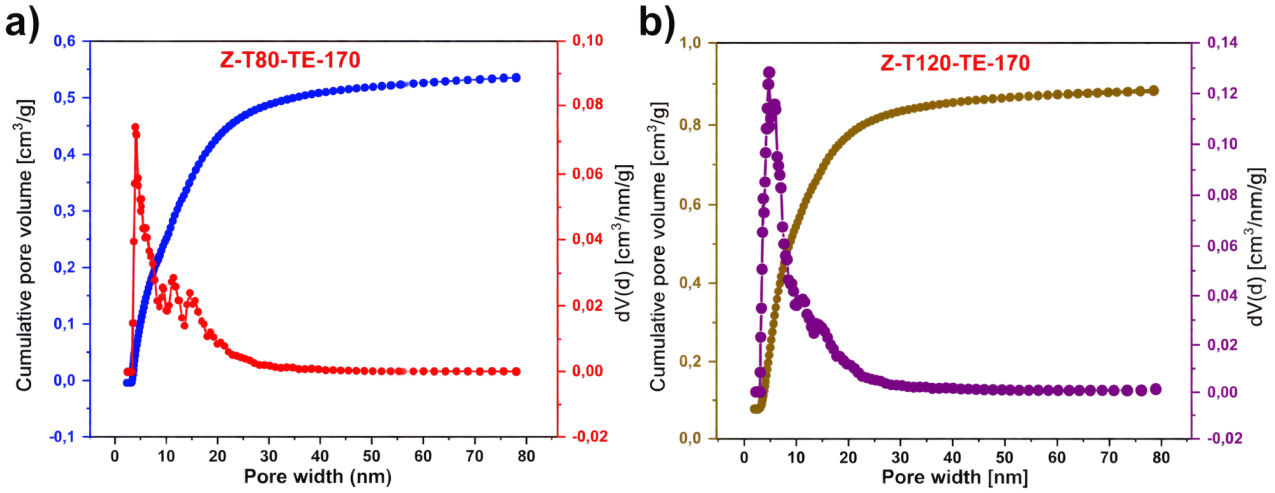


FIGURE 4. Pore volume distribution of the MFI-type ZSM-5

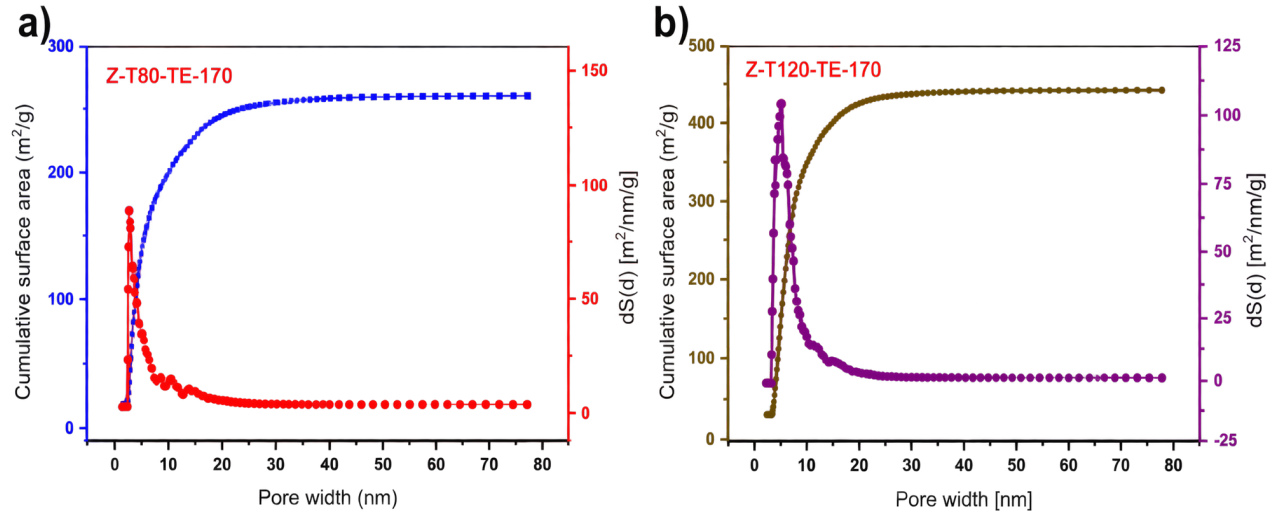


FIGURE 5. Surface area distribution of the MFI-type ZSM-5

The results obtained from the NLDFT analysis of both samples can be compared in Figure 5**.** The pore size distribution profiles (BJH differential surface area dS(d) and pore volume dV(d) vs. pore width) support this picture: both samples show their dominant differential contribution concentrated in the small mesopore range (~2-6 nm), with cumulative surface area reaching a plateau by approximately 20 nm pore width in both cases, while cumulative pore volume continues to rise gradually out to ~40-80 nm, reflecting a broader distribution of larger mesopores that contribute proportionally more volume than surface area. The peak differential surface area and pore volume are both substantially larger in magnitude for Z-T120-TE-170 than Z-T80-TE-170, consistent with its higher overall BET/BJH/DFT surface area and pore volume.

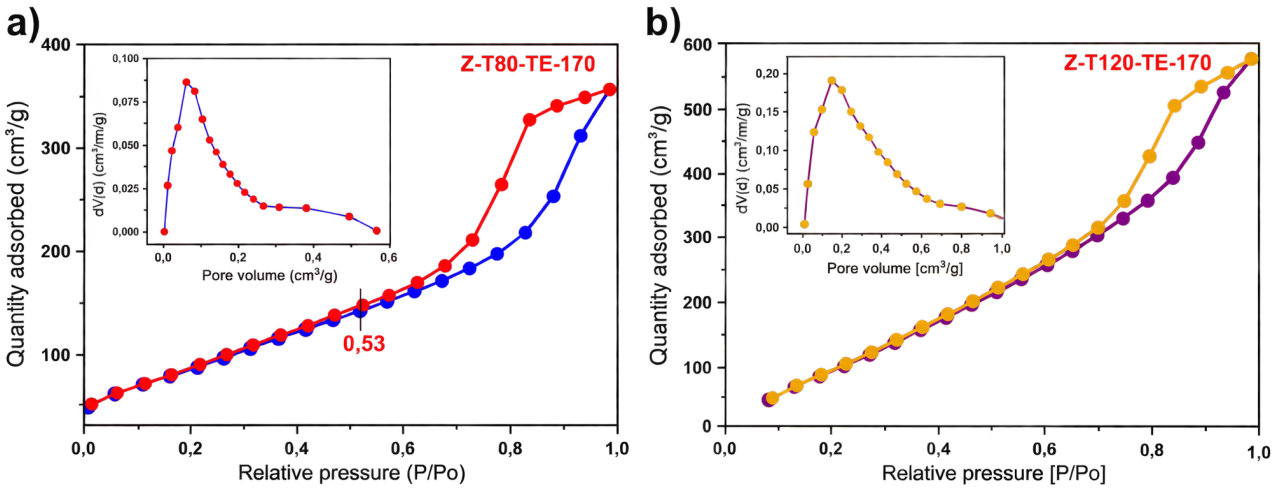


FIGURE 6. Nitrogen adsorption-desorption isotherm of the MFI-type ZSM-5

Figure 6 presents a qualitative difference between the two samples, not evident from the summary textural parameters alone, that emerges on inspection of the full isotherms. Z-T80-TE-170 exhibits a Type IV(a) isotherm with a clearly resolved H2-type hysteresis loop, with the adsorption and desorption branches diverging over the range P/Po ≈ 0.5-0.95 and the loop closing at P/Po ≈ 0.53. This closure point is close to, though somewhat higher than, the classical tensile-strength-effect (TSE) closure point (P/Po ≈ 0.42 for N_2 at 77 K) below which artificial forced closure is expected; an H2-type loop of this kind is typically associated with pore networks featuring pore-blocking effects, such as interconnected pores with narrow necks and wider bodies [22], [23]. In marked contrast, Z-T120-TE-170 shows an isotherm in which the adsorption and desorption branches are nearly coincident across almost the entire relative pressure range, with only a very narrow, low-amplitude separation near saturation (P/Po > 0.75). This near-absence of hysteresis is inconsistent with a well-defined, confined intracrystalline mesopore network of the ink-bottle type, and is more characteristic of adsorption on loosely packed, non-confined interparticle voids between primary particles or aggregates often described as textural porosity [3], [24], [25].

This observation directly helps explain the t-Plot anomaly flagged in Table 2, pore structure dominated by open interparticle voids, rather than confined intracrystalline mesopores, would not produce the sharp micropore-filling step at very low relative pressure that the t-Plot method relies on to separate micropore from external/mesopore contributions, consistent with the near-zero t-Plot micropore volume/area reported for Z-T120-TE-170, without requiring any loss of the underlying MFI microporous framework itself, which XRD and FTIR confirm.

4. Conclusion

ZSM-5 samples with Si/Al molar ratios of 80 (Z-T80-TE-170) and 120 (Z-T120-TE-170) were successfully synthesized at a fixed crystallization temperature of 170°C, with formation of the MFI framework confirmed independently by XRD (characteristic reflections at 2θ ≈ 7.9-8.0°, 8.9°, 23.1-23.2°, and 23.9-24.1°, indexed to the (101), (200), (332), and (303) planes) and FTIR (double-ring band at 559-561 cm^{-1}, diagnostic of the MFI five-membered-ring building units). The Si/Al ratio variation instead manifests primarily in the internal asymmetric T-O-T stretching band, which shifts from 1057.0 cm^{-1} (Si/Al = 80) to 1072.5 cm^{-1} (Si/Al = 120), consistent with reduced framework aluminum content increasing the proportion of shorter, stiffer Si-O-Si linkages relative to Si-O-Al linkages. Textural properties differ substantially between the two samples despite

their similar crystalline framework: increasing the Si/Al ratio from 80 to 120 nearly doubles the BET surface area (323.5 → 566.7 m²/g) and increases the DFT pore volume (0.537 → 0.871 cc/g) and DFT mode pore width (3.54 → 4.89 nm). The two samples display qualitatively different N_2 isotherm hysteresis behavior, a clearly resolved H2-type loop for Z-T80-TE-170 (closure at P/Po ≈ 0.53) versus a near-absence of hysteresis for Z-T120-TE-170 — suggesting a shift from confined, ink-bottle-type mesoporosity toward more open, interparticle (textural) porosity at the higher Si/Al ratio; this interpretation is consistent with, and offers a plausible explanation for, the near-zero t-Plot micropore contribution observed for Z-T120-TE-170, without implying loss of the underlying microporous MFI framework

Acknowledgements

The authors gratefully acknowledge the financial support provided through the International Collaborative Research (Penelitian Kerjasama Internasional, PKSI) scheme by the Center for Research and Community Service (Pusat Penelitian dan Pengabdian kepada Masyarakat, P3M), Politeknik Negeri Ujung Pandang, under Research Contract No. 1334/P/2026. The authors also sincerely appreciate the institutional support provided throughout the implementation of this research.

Data Availability Statement

The raw and processed data supporting the findings of this study, including X-ray diffraction (XRD), Fourier-transform infrared spectroscopy (FTIR), and nitrogen adsorption–desorption (BET) data, are available from the corresponding author upon reasonable request.

Funding

This research was funded by the International Collaborative Research (PKSI) scheme of the Center for Research and Community Service (P3M), Politeknik Negeri Ujung Pandang, under Research Contract No. 1334/P/2026.

References

[1] T. F. Degnan, G. K. Chitnis, and P. H. Schipper, “History of ZSM-5 fluid catalytic cracking additive development at Mobil,” *Microporous and Mesoporous Materials*, vol. 35–36, pp. 245–252, Apr. 2000, doi: 10.1016/S1387-1811(99)00225-5.

[2] C. Zhou, C. Han, X. Min, and T. Yang, “Effect of different sulfur precursors on efficient chromium(VI) removal by ZSM-5 zeolite supporting sulfide nano zero-valent iron,” *Chemical Engineering Journal*, vol. 427, p. 131515, Jan. 2022, doi: 10.1016/j.cej.2021.131515.

[3] H. Jia *et al.*, “Synthesis of Template-Free ZSM-5 from Rice Husk Ash at Low Temperatures and Its CO2 Adsorption Performance,” *ACS Omega*, vol. 6, no. 5, pp. 3961–3972, Feb. 2021, doi: 10.1021/acsomega.0c05842.

[4] S. Sivalingam and S. Sen, “Rice husk ash derived nanocrystalline ZSM-5 for highly efficient removal of a toxic textile dye,” *Journal of Materials Research and Technology*, vol. 9, no. 6, pp. 14853–14864, Nov. 2020, doi: 10.1016/j.jmrt.2020.10.074.

[5] Z. Sun, T. Hu, Y. Pan, Z. Liu, and C. Wu, “Preparation and performance of platinum catalysts for hydrosilylation supported by polyphenols modified SBA-15,” *J Porous Mater*, Jul. 2026, doi: 10.1007/s10934-026-01944-9.

[6] R. J. Argauer and G. R. Landolt, “Crystalline zeolite zsm-5 and method of preparing the same,” US3702886A, Nov. 14, 1972 Accessed: Sep. 12, 2026. [Online]. Available: https://patents.google.com/patent/US3702886A/en

[7] K. Egeblad, C. H. Christensen, M. Kustova, and C. H. Christensen, "Templating Mesoporous Zeolites", Accessed: Jul. 26, 2026. [Online]. Available: https://dx.doi.org/10.1021/cm702224p
[8] H. Wang *et al.*, "Hierarchically porous zeolites synthesized with carbon materials as templates," *Front. Chem. Sci. Eng.*, vol. 15, no. 6, pp. 1444–1461, Dec. 2021, doi: 10.1007/s11705-021-2090-6.
[9] C. S. Cundy and P. A. Cox, "The Hydrothermal Synthesis of Zeolites: History and Development from the Earliest Days to the Present Time," *Chem. Rev.*, vol. 103, no. 3, pp. 663–702, Mar. 2003, doi: 10.1021/cr020060i.
[10] X. Chen, R. Jiang, Y. Gao, Z. Zhou, and X. Wang, "Synthesis of nano-ZSM-5 zeolite via a dry gel conversion crystallization process and its application in MTO reaction," *CrystEngComm*, vol. 23, no. 15, pp. 2793–2800, Apr. 2021, doi: 10.1039/D1CE00162K.
[11] C. S. Cundy and P. A. Cox, "The hydrothermal synthesis of zeolites: Precursors, intermediates and reaction mechanism," *Microporous and Mesoporous Materials*, vol. 82, no. 1, pp. 1–78, Jul. 2005, doi: 10.1016/j.micromeso.2005.02.016.
[12] S. Bosnar *et al.*, "Overcoming phase separation in dual templating: A homogeneous hierarchical ZSM-5 zeolite with flower-like morphology, synthesis and in-depth acidity study," *Microporous and Mesoporous Materials*, vol. 329, p. 111534, Jan. 2022, doi: 10.1016/j.micromeso.2021.111534.
[13] M. Guo *et al.*, "Aging Characteristics of ZSM-5 Zeolite on Low-Frequency Acoustic Applications," *Nanomaterials*, vol. 15, no. 9, Art. no. 9, Jan. 2025, doi: 10.3390/nano15090639.
[14] F. Wang *et al.*, "ZSM-5/Y composite zeolite enabled via ZSM-5 refabrication and outstanding performance of the composite in VGO catalytic cracking," *Chemical Engineering Journal*, vol. 519, p. 165476, Sep. 2025, doi: 10.1016/j.cej.2025.165476.
[15] K. L. A. Cao *et al.*, "Preparation of Hierarchical Porous Zeolite Particles with Multiscale Pore Architectures through a Template-Assisted Spray Process for Enhanced Toluene Adsorption Rate," *ACS Appl. Mater. Interfaces*, vol. 17, no. 16, pp. 24310–24326, Apr. 2025, doi: 10.1021/acsami.4c22163.
[16] Y. Wang and A. Tuel, "Nanoporous zeolite single crystals: ZSM-5 nanoboxes with uniform intracrystalline hollow structures," *Microporous and Mesoporous Materials*, vol. 113, no. 1, pp. 286–295, Aug. 2008, doi: 10.1016/j.micromeso.2007.11.027.
[17] A. Zhang, L. Wang, W. Wang, S. Liu, and H. Long, "Preparation of mesoporous ZSM-5s via a dual templating approach," *Inorganic Chemistry Communications*, vol. 189, p. 116773, Jul. 2026, doi: 10.1016/j.inoche.2026.116773.
[18] Y. Ouyang *et al.*, "Synthesis of Hierarchical Hollow ZSM-5 Zeolite Crystals by the Synergistic Effect of Dual Etching Agents for Dye Adsorption," *Inorg. Chem.*, vol. 64, no. 24, pp. 12086–12099, Jun. 2025, doi: 10.1021/acs.inorgchem.5c01397.
[19] J. C. Jansen, F. J. van der Gaag, and H. van Bekkum, "Identification of ZSM-type and other 5-ring containing zeolites by i.r. spectroscopy," *Zeolites*, vol. 4, no. 4, pp. 369–372, Oct. 1984, doi: 10.1016/0144-2449(84)90013-7.
[20] E. M. Flanigen, H. Khatami, and H. A. Szymanski, "Infrared Structural Studies of Zeolite Frameworks," in *Molecular Sieve Zeolites-I*, vol. 101, in Advances in Chemistry, no. 101, vol. 101, American Chemical Society, 1974, pp. 201–229. doi: 10.1021/ba-1971-0101.ch016.
[21] F. Wang *et al.*, "Solvent- and metal-free upcycling of low-density polyethylene using a practical ZSM-5/Al2O3 bead catalyst," *Commun Chem*, vol. 9, no. 1, p. 166, Apr. 2026, doi: 10.1038/s42004-026-02039-x.
[22] M. Thommes *et al.*, "Physisorption of gases, with special reference to the evaluation of surface area and pore size distribution (IUPAC Technical Report)," *Pure and Applied Chemistry*, vol. 87, no. 9–10, pp. 1051–1069, Oct. 2015, doi: 10.1515/pac-2014-1117.
[23] K. Ishizaki, S. Komarneni, and M. Nanko, "Properties and evaluation techniques for porous materials," in *Porous Materials*, in Materials Technology Series. , Springer, Boston, MA, 1998, pp. 202–224. doi: 10.1007/978-1-4615-5811-8_6.

[24] R. Thahir *et al.*, "Engineered dual-template SBA-15/Fe_3O_4 nanocomposites: Mesoporous structure and magnetically recoverable adsorbents for Pb(II) and synthetic dye removal," *Next Materials*, vol. 11, p. 101764, Apr. 2026, doi: 10.1016/j.nxmate.2026.101764.

[25] M. Hartmann, M. Thommes, and W. Schwieger, "Hierarchically-Ordered Zeolites: A Critical Assessment," *Advanced Materials Interfaces*, vol. 8, no. 4, p. 2001841, 2021, doi: 10.1002/admi.202001841.